the Ag(I) analogue **2** would be consistent with the ordering of the d → s energies of the mononuclear free ions (above), but the differences are much smaller. Ligand coordination would be expected to raise s-orbital energies substantially, but the effect of metal–metal interactions in the $(M^I)_6$ octahedra would lead to substantial splitting of the d and (especially s) orbitals in a manner which may lead to marked effects on the expected molecular orbital energies. A diagram representing the resulting cluster metal MO's is displayed in Figure 7 and illustrates the stabilization of the lowest energy unfilled s orbital and corresponding destabilization of the highest energy filled d orbital. It is likely that the metal–metal interactions in the silver clusters are substantially greater than in the respective copper cluster because, relative to the sums of their respective van der Waals radii, the Ag–Ag distances, especially in **2** but also in **3**, are significantly shorter than the Cu–Cu distance in **1**. This enhanced interaction should decrease the d → s separation accordingly.

Earlier studies from these two laboratories[2,3] have identified strong, low-energy emission bands in the luminescence spectra of the Cu(I) cluster $Cu_4I_4(py)_4$ (**4**) and a series of related $Cu_4I_4L_4$ analogues where L is either a saturated or aromatic amine. Recent ab initio calculations[26] have concluded that the emitting excited state can be viewed to be of mixed character consisting of roughly equal parts of iodide to copper charge transfer (XMCT, X = I) and metal-centered d → s contributions, the energies markedly influenced by the metal–metal interactions in the excited state. Blasse[27] has reached a similar conclusion. The idea of mixed d → s/XMCT character of electronic transitions was advanced some years ago by Jørgensen[28] to explain the absorption spectra of Cu(I) and Ag(I) halide salts. For example, when Ag^+ is doped into alkali metal halides (X^-), the longest wavelength "d → s" transition follows the energy order $Cl^- > Br^- > I^-$. The iodide salts show the largest shift to lower energy due to greater mixing of the metal d orbitals with the halide p orbitals and, hence, a greater LMCT contribution to the transition.

Also relevant to the present discussion is a self-consistent charge and configuration MO investigation[29] of Cu(I) clusters of the type having a $Cu_8S_{12}^{4-}$ core with the eight coppers in a cubane configuration with Cu–Cu distances of 2.83 Å and the sulfurs coming from bidentate ions such as 1,1-dicyanoethylene-2,2-dithiolate. This study concluded that the HOMO's are largely sulfur in character while the LUMO is primarily copper 4s and 4p and sulfur 3p orbitals. These results would imply that the HOMO's for the octahedral clusters described in the present case are also largely ligand in character. However, the ab initio calculations described for the Cu(I) tetrahedra[26a] clearly indicate considerable ground-state charge delocalization from ligand anions to the metal core and much less than a full electron transfer from ligand to metal in the lowest energy excited state. Thus, in such a case, viewing the ES conveniently as simply the product of a one-electron HOMO → LUMO transition may present an incomplete picture of the changes wrought by the electronic excitation.

In the context of the calculations described above for $Cu_4I_4(py)_4$, a "cluster-centered" (CC) state with both d → s and LMCT character would appear to be an accurate, although qualitative, description of the luminactive excited states of **1–3**. The a_{1g} lowest unoccupied MO of the $(M^I)_6$ octahedra (Figure 7) would be largely metal s orbital in character and would be a bonding MO with respect to the metal–metal interactions. Therefore, a d → s transition, a LMCT transition, or the presumed CC transition of mixed character would lead to population of this orbital with a resulting contraction of the $(M^I)_6$ octahedron. Such a distortion would be one factor accounting for the large Stokes shift from the excitation maxima to the emission maxima of the two monothiocarcarbamate complexes **1** and **2**. We do not have as ready an explanation for the smaller, but still substantial, Stokes shift for **3**, although it should be noted that, in the ground state for this species, the $(M^I)_6$ core is already significantly distorted from the nearly regular octahedra which characterize the other two. The relatively long emission lifetimes at 77 K for **1–3** (Table III) are consistent with those expected for a spin-forbidden transition in such metal complexes. The emitting state is thus concluded to be a triplet CC ES of mixed d → s and LMCT character.

Acknowledgment. This research was supported by the Deutsche Forschungsgemeinschaft (Grant Vo 211/9-1) and the U.S. National Science Foundation (Grant CHE 87-22561). F.S. gratefully acknowledges a travel grant from the German Academic Exchange Service (daad). We thank Dr. N. L. Keder of UCSB for her help in recording and interpreting X-ray powder diffraction data.

(26) (a) Vitale, M.; Palke, W. E.; Ford, P. C. Submitted for publication. (b) Kyle, K. R.; Palke, W. E.; Ford, P. C. *Coord. Chem. Rev.* **1990**, *97*, 35–46.
(27) Blasse, G. *Struct. Bonding* **1991**, *76*, 153–187.
(28) Jørgensen, C. K. *Oxidation Numbers and Oxidation States*; Springer Verlag: New York, 1969; p 128.
(29) Avdeef, A.; Fackler, J. P., Jr. *Inorg. Chem.* **1978**, *17*, 2182–2187.
(30) Mingos, D. M. P. *J. Chem. Soc., Dalton Trans.* **1976**, 1163–1169.

Contribution from the Institute of Chemical Engineering and High Temperature Chemical Processes and Department of Chemical Engineering, University of Patras, P.O. Box 1239, GR-26110 Patras, Greece

Raman Spectroscopic Studies of Metal–Metal Halide Molten Mixtures: The Mercury–Mercury(II) Halide Systems

G. A. Voyiatzis and G. N. Papatheodorou*

Received April 9, 1991

Raman spectra of molten HgX_2–Hg (X = Cl, Br, I) systems have been obtained at compositions up to 30 mol % in Hg from 550 to 818 K. The dissolution of mercury in mercury halides gives rise to resonance-enhanced Raman bands which were interpreted to account for Hg_2X_2 type molecular species formed in all mercury compositions and Hg_3X_2 type molecules formed at high mercury mole fractions. Spectra were also obtained from HgX_2–HgX'_2–Hg (X = F, Cl, Br, I) mixtures and were attributed to mixed mercury(I) (sub)halide molecules Hg_2XX' formed in the melt. The Hg_2X_2 and Hg_2XX' molecules possess a linear symmetry, and the Hg–Hg stretching frequencies for all 10 molecules were found to be between ~180 cm^{-1} (Hg_2F_2) and ~100 cm^{-1} (Hg_2I_2). A linear Hg_3 chain is formed in the Hg_3X_2 molecules bound to two terminal halides. The formation of Hg_3 chains was further confirmed by the Raman spectra of $Hg_3(AlCl_4)_2$ melts. It is suggested that in the melt mixtures intermolecular interactions between HgX_2 and Hg_2X_2 molecules lead to an alteration of oxidation states which account for a "hopping" like conduction.

Introduction

At elevated temperatures many metals are to some extent soluble in their molten halide salts, forming, in most cases, colored solutions. The basic physical properties and the equilibrium phase diagrams of a large number of metal–metal halide (M–MX_n) systems were determined in the 1960s, and most of this work was summarized in reviews by Bredig[1] and Corbett.[2] Some interesting

(1) Bredig, M. A. In *Molten Salt Chemistry*; Blander, M., Ed.; Interscience: New York, 1964; p 367–425.

0020-1669/92/1331-1945$03.00/0

Table I. Visual Observations Made and Laser Lines Used

molten syst	color (at ~20 °C above melting)	laser line, nm
$HgCl_2$	colorless transparent	Ar^+, Kr^+
$HgCl_2$–Hg	tint green ($X_{Hg} \sim 0.04$), yellow ($X_{Hg} \sim 0.15$), black red ($X_{Hg} \sim 0.3$)	514.5 and all Kr^+; 676.4 for $X_{Hg} \sim 0.3$
$HgBr_2$	tint green, transparent	514.5 and all Kr^+
$HgBr_2$–Hg	as in $HgCl_2$–Hg but darker colors	all Kr^+; 676.4 for high Hg concentration
HgI_2	deep red, transparent	676.4
HgI_2–Hg	black red ($X_{Hg} \sim 0.02$), opaque black ($X_{Hg} \sim 0.1$ to 0.3)	676.4 and back-scattering
HgF_2–HgX_2–Hg	as for the HgX_2–Hg systems	676.4 and back-scattering
HgX_2–HgX'_2	combination of colors of individual salts	514.5 (X, X' = Cl, Br), 647.1 (X, X' = Cl, I), 676.4 (X, X' = Br, I)
HgX_2–HgX'_2–Hg	combinations of colors of HgX_2–Hg systems	Kr^+
$Hg_3(AlCl_4)_2$	almost black	676.4 and back-scattering

phenomena such as electron localization in ionic media and electron transport, metal–nonmetal transition, and liquid–liquid-phase separation, that many M–MX_n liquid mixtures exhibit, were studied spectroscopically by means of optical absorption, NMR spectroscopy, ESR spectroscopy, and neutron scattering. Most of this work regarding the alkali metal–alkali-metal halide and bismuth–bismuth halide solutions has been reviewed by Warren.[3,4] The thermodynamic and physical properties such as electrical conductivity and magnetic susceptibility have also been reviewed[5] for a variety of M–MX_n systems. Recently, the electrochemical properties of dissolved metals in molten salts, including migration, anodic oxidation, and electronic conductivity, have also been reviewed.[6,7]

The metal solubilities in the M–MX_n systems vary markedly throughout the periodic table, and there is no systematic dependence on "ionic" or "molecular" character of the host molten salt solvent. Spectroscopic studies related to the structure of the "metal species" formed as well as the overall structure of the mixture are very limited. Neutron-scattering experiments have been carried out in certain alkali metal–alkali-metal halide systems,[8] and Raman measurements have been reported in the In–InX_3 (X = Cl, Br)[9] and the Cd–$Cd(AlCl_4)_2$[10] systems. For the indium systems the presence of In^+ and InX_4^- ions has been established, while for the cadmium system a Cd–Cd metal bond has been argued to be present.[10,12]

The solubility[1,2] of Hg in the molecular-like HgX_2 melts[11-13] is high, leading finally to the precipitation of solid Hg_2X_2 compounds, and thus a wide range of compositions can be studied. Freezing point depression measurements,[14] electromotive force measurements,[15] and electrical conductivity measurements[16] for the HgX_2–Hg molten system suggested that Hg dissolves either as atoms,[14,15] as Hg_2X_2 molecules,[14] or as cation dimers Hg_2^{2+}.[15,16]

The purpose of the present work is to investigate the structural properties of the mercury species formed by dissolution of mercury metal in mercury(II) halide melts. Liquid HgX_2–Hg (X = Cl, Br, I) mixtures as well as mixed mercury halide–mercury systems HgX_2–HgX'_2–Hg (X ≠ X'; X, X' = F, Cl, Br, I) have been examined by Raman spectroscopy at temperatures up to 818 K. The data obtained for all systems were interpreted to indicate the formation of molecular subhalides (Hg_2X_2, Hg_3X_2, Hg_2XX') of mercury which could be mixed with the HgX_2 solvent, forming molecular mixtures.

The notations HgX_2–Hg and HgX_2–HgX'_2-Hg are used in this paper, but it should be understood that these formulas represent only the stoichiometry of the initial mixtures and are not indicative of the species and oxidation states present. The compositions of the mixtures are expressed in terms of mole fraction of dissolved mercury metal, X_{Hg}.

Experimental Section

High-purity anhydrous $HgCl_2$ and $HgBr_2$ were prepared from the corresponding pa Merck and Riedel-de Haen reagents by heating for 3 h at 383 K under dynamic vacuum and then by vapor transport in evacuated and sealed fused-silica tubes. Slow vacuum sublimations were used for the purification of the HgI_2 (pa Merck) reagent in sealed Pyrex tubes. Mercurous halides (Hg_2X_2; X = Cl, Br, I) were prepared by mixing and heating together (at 558 K for Cl and Br, and at 543 K for I) for 24 h the appropriate amounts of mercuric halides and mercury metal (pa Merck) in fused-silica tubes. Mercuric fluoride was purchased from Cerac Pure and used without further purification. Aluminum chloride (Fluka AG) was purified by repeated slow vapor transport under a narrow thermal gradient (~30 °C around the $AlCl_3$ melting point) in sealed Pyrex tubes under vacuum. After 10 h, oxide clear $AlCl_3$ crystals were obtained in the cold zone. The $Hg_3(AlCl_4)_2$ yellow compound was prepared by mixing and heating together at 550 K for 3 days the appropriate amounts of $HgCl_2$, Hg, and $AlCl_3$ (1:2:2). At 485 K, $Hg_3(AlCl_4)_2$ was an almost black viscous melt. The anhydrous materials were handled in Pyrex tubes sealed in vacuo or in a N_2-atmosphere drybox with a water vapor content of less than 1 ppm where all material transfers took place. Hg_2X_2 (X = Cl, Br, I) reagents were also protected from light.

Raman cells were made of fused-silica tubing: 3-mm i.d., 4-mm o.d., and 30-mm length. All cells were thoroughly cleaned, baked out to red-heat, and degassed by evacuating while hot. The total amount of chemicals added to the cells was approximately 180 mg. Calculated amounts of Hg metal were first added in the cell, and then the cell was placed into the glovebox for adding mercury(II) halide(s). Alternatively, instead of Hg, the subhalides of Hg_2X_2 (X = Cl, Br, I) were prepared and used for making the appropriate mixtures with a known HgX_2:Hg composition. Raman spectra measurements from different cells containing the same molten salt (HgX_2) to metal (Hg) composition, but prepared by the addition of either Hg or Hg_2X_2, were found to be identical. The compositions studied for the HgX_2–Hg systems were $0 < X_{Hg} < 0.33$, which lie within the mole fraction range $0 < X_{Hg_2X_2} < 0.5$ of the equivalent description of the systems as HgX_2–Hg_2X_2. All cells containing the chemicals were placed on a vacuum line, then cooled at their bottom in liquid N_2, and sealed with a butane torch. In order to limit the fluoride attack on the fused-silica cell, only cells with mixed HgF_2–HgX_2 (X = Cl, Br, I) were prepared containing different amounts of Hg but having HgF_2 mole fractions less than 0.4.

Each cell was heated in a Nichrome-wound optical furnace, and the chemicals were melted and kept above the liquids at different time in-

(2) Corbett, J. D. In *Fused Salt*; Sundeim, B., Ed.; McGrawHill: New York, 1964; p 341–407.
(3) Warren, W. W., Jr. In *The Metallic and Nonmetallic States of Matter*; Edwards, P. P., Rao, C. N. R., Eds.; Taylor and Francis: London, 1985; p 139–168.
(4) Warren, W. W., Jr. In *Molten Salt Chemistry*; Mamantov, G.; Marassi, R., Eds.; D. Reidel Publishing Co.: Dordrecht, The Netherlands, 1987; p 237–257.
(5) Warren, W. W., Jr. In *Advances in Molten Salt Chemistry*; Mamantov, G., Braunstein, J., Eds.; Plenum: New York, 1981; Vol. 4, p 1–69.
(6) Haarberg, G. M. Thesis, University of Trondheim, Trondheim, Norway, 1985.
(7) Haarberg, G. M.; Thonstad, J. *J. Appl. Electrochem.* **1989**, *19*, 789.
(8) (a) Chabrier, G.; Jal, J. F.; Chieux, P.; Dupuy, J. *Phys. Lett.* **1982**, *93A*, 47. (b) Jal, J. F.; Dupuy, J.; Chieux, P. *J. Phys. C: Solid State Phys.* **1985**, *18*, 1347.
(9) Radloff, P. F.; Papatheodorou, G. N. *J. Chem. Phys.* **1980**, *72*, 992.
(10) Corbett, J. D.; Burkhard, W. J.; Druding, L. F. *J. Am. Chem. Soc.* **1961**, *83*, 76.
(11) Brooker, M. H.; Papatheodorou, G. N. In *Advances in Molten Salt Chemistry*; Mamantov, G., Mamantov, C. B., Eds.; Elsevier: New York, 1983, Vol. 5, p 27–184.
(12) Voyiatzis, G. A.; Papatheodorou, G. N. *Proc.—Electrochem. Soc.* **1990**, *90–17*, 161–173.
(13) Voyiatzis, G. A.; Papatheodorou, G. N. To be published.
(14) Yosim, S. J.; Mayer, S. W. *J. Phys. Chem.* **1960**, *64*, 909.
(15) Topol, L. E. *J. Phys. Chem.* **1963**, *67*, 2222.
(16) Grantham, L. F. *J. Chem. Phys.* **1968**, *49*, 3835.

Table II. Observed[a] Raman Frequencies (cm^{-1}) for HgX_2–Hg Melts[b]

$HgCl_2$–Hg	$HgBr_2$–Hg	HgI_2–Hg	assgnt[c]		
		Solvent[d]			
375 (dp) [0.7][e]	260 (dp) [0.7]	205 (dp) [0.7]	HgX_2	(B_{2g})	ant. stretch
324 (dp)	202 (dp)	143 (dp)	HgX_2	(B_{2g})	
310[f] (p) [0.02]	194[f] (p) [0.02]	137[f] (p) [0.02]	HgX_2	ν_1^S (A_g)	Hg–X sym stretch
(108) (dp)	(78) (dp)		HgX_2[g]		
(55) (dp)	(40) (dp)	(32) (dp)	HgX_2[g]		
		Low Hg Content			
(260) (vw, sh)	223 (vw)	183 (vw, sh)	Hg_2X_2	ν_1^P (Σ_g^+)	Hg–X stretch
{279}[h]	{220}[h]	{194}[h]			
154[i] (p) [0.21]	124[i] (p) [0.21]	100[i] (p) [0.21]	Hg_2X_2	ν_2^P (Σ_g^+)	Hg–Hg stretch
{166}[j]	{134}[j]	{113}[j]			
		High Hg Content			
100 (p)	87 (p)	(80) (p)	Hg_3X_2	ν^T (Σ_g^+)	Hg–Hg–Hg stretch

[a] Key: p = polarized, dp = depolarized, vw = very weak, sh = shoulder. [b] The values listed here were measured a few degrees above melting. [c] Details on solvent band assignments are in ref 13. [d] Position and half-widths of solvent bands are temperature dependent.[13] [e] Depolarization ratios are in brackets. [f] Exhibits blue shift with increasing temperature[13] and red shift with increasing Hg content. [g] Bands on Rayleigh wing due to reorientational motions.[13] [h] Hg–X stretching in solid Hg_2X_2.[33,34] [i] Exhibits small red shift with increasing Hg content. [j] Hg–Hg stretching in solid Hg_2X_2.[33,34]

tervals. The color of melt was observed, and the possible attack on the cell walls was systematically checked at different temperatures above the liquids. The knowledge of the color of the melt was important for choosing the appropriate laser line. The coloration of the liquids ranged from a clear transparent melt for pure $HgCl_2$ to black-red or black liquids for certain mixtures with high metal content. Table I summarizes the general features of the colors observed for the different liquids. For all systems studied here, increasing temperature gives rise to an intensified coloration of the melts. No essential differences in the corresponding Raman spectra arose from this effect. Only a slight lowering of relative Raman intensities and a relative increase in the bandwidths was observed.

Raman spectra were excited with a Spectra Physics argon or krypton ion laser. The scattered light was analyzed with a Spex 1403 double monochromator and PAR (SSR) photon-counting electronics. Both 90° and back-scattering geometries have been used, as indicated in Table I. An optical furnace with adjustable temperature gradient was used. The optical cells for molten salt samples were placed in a mechanically stable metal block inside the optical furnace and were always in a fixed position relative to the collecting lens and/or the entrance slit. The optical furnace and experimental setup, as well as the procedures and techniques for obtaining Raman spectra at elevated temperatures have been previously described.[10,17]

Results and Discussion

The Raman spectra of over 50 cells containing the HgX_2–Hg and HgX_2–HgX'_2–Hg molten mixtures at different metal compositions have been successfully measured at different temperatures. Figures 1–3 show representative spectra for the HgX_2–Hg molten mixtures as well as for the pure solvent melts. For all compositions studied, the Raman spectra were a superposition of the HgX_2 solvent bands plus a new strong and polarized band at 154, 124, and 100 cm^{-1} in the chloride, bromide, and iodide systems, respectively. Other weaker bands due to the dissolved metal have also been observed at higher amplifications of the Raman signal, while for high mercury metal contents ($X_{Hg} > 0.15$) a new band at lower frequencies is also present for all systems. The intensities of the bands due to small additions of mercury metal ($X_{Hg} < 0.05$) are high relative to the HgX_2 solvent bands, indicating a resonance Raman enhancement.[18] The depolarization ratio of the solute bands have values near 0.2 (Table II), which are expected from solutions exhibiting resonance enhancement of their bands with A_g or Σ_g^+ symmetry.[18] Table II gives a summary of the frequencies of all bands observed and an assignment based on the discussion that follows.

It is known that, in the solid state, $HgCl_2$, $HgBr_2$, and the yellow form of HgI_2 form molecular crystals containing the approximately linear X–Hg–X molecules.[19–21] In the vapor (gaseous) state electron diffraction[22–24] and vibrational spectroscopy[25–27] have

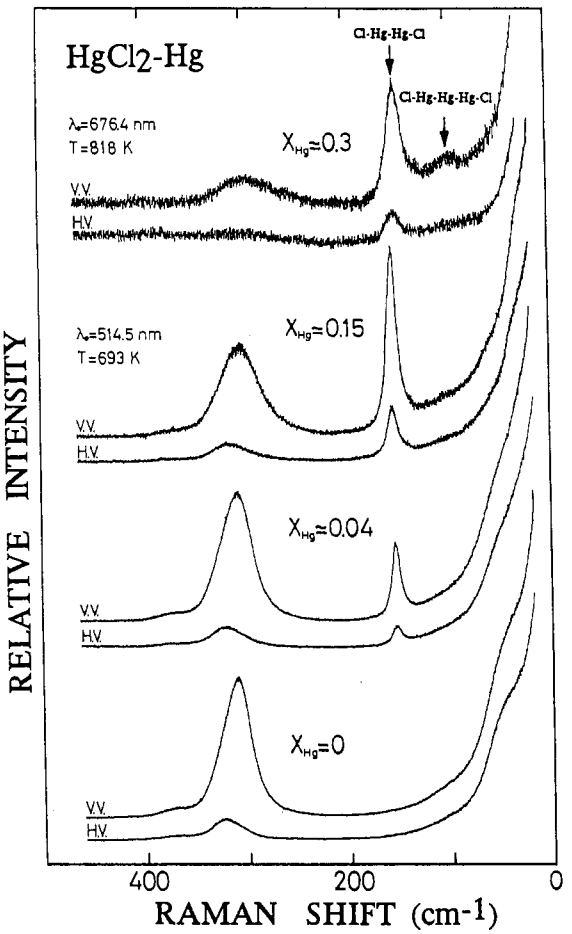

Figure 1. Raman spectra of the $HgCl_2$–Hg molten system. $O \leq X_{Hg} \leq 0.15$: power (P) = 40 mW, spectral slit width (SSW) ~ 1.5 cm^{-1}, time constant (τ) = 0.1 s. $X_{Hg} \approx 0.3$: P = 50 mW, SSW ~ 3.5, τ = 0.3 s. Scan rate (SR) = 30 cm^{-1} min^{-1}. VV indicates that incident and scattered radiation is polarized perpendicular to the scattering plane. HV indicates that incident radiation is polarized *in* the scattering plane and the scattered radiation analyzed *perpendicular to* the scattering plane.

(17) Boghosian, S.; Papatheodorou, G. N. *J. Phys. Chem.* **1989**, *93*, 415.
(18) (a) Clark, R. J. H. In *Advances in Infrared and Raman Spectroscopy*; Clark, R. J. H., Hester, R. E., Eds.; Heyden: New York, 1975; Vol. 1, p 143–172. (b) Clark, R. J. H. In *Advances in Infrared and Raman Spectroscopy*; Clark, R. J. H., Hester, R. E., Eds.; Wiley: New York, 1984, Vol. 11, p 95–132.
(19) Subramanian, V.; Seff, K. *Acta Crystallogr.* **1980**, *B36*, 2132.
(20) Braekken, H. *Z. Kristallogr.* **1932**, 81.
(21) Jeffrey, G. A.; Vlasse, M. *Inorg. Chem.* **1967**, *6*, 393.
(22) Kashiwubara, K.; Konaka, S.; Kimura, M. *Bull. Chem. Soc. Jpn.* **1973**, *46*, 410.

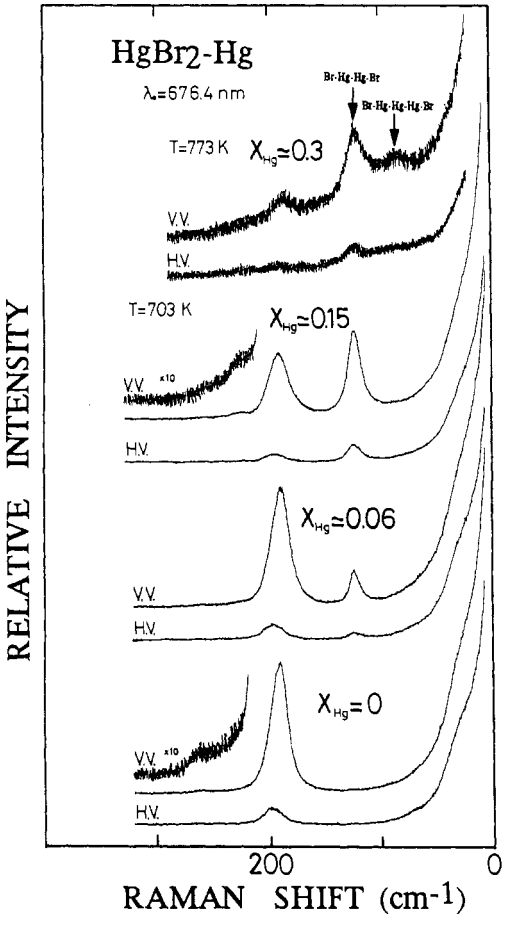

Figure 2. Raman spectra of the $HgBr_2$–Hg molten system: P = 50 mW (X_{Hg} = 0, $X_{Hg} \approx 0.06$); P = 100 mW ($X_{Hg} \approx 0.15$, $X_{Hg} \approx 0.3$); SSW ~ 2 (SSW ~ 3.5 for $X_{Hg} \approx 0.3$); τ = 0.3 s; SR = 30 cm^{-1} min^{-1}.

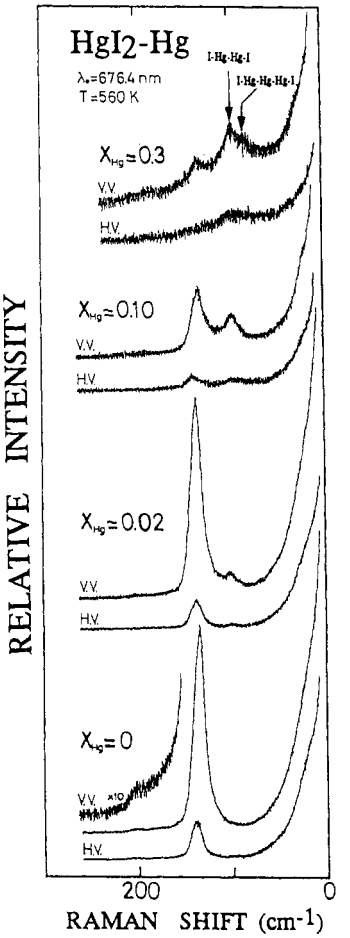

Figure 3. Raman spectra of the HgI_2–Hg molten system. X_{Hg} = 0: P = 30 mW, SSW ~ 2, τ = 0.1 s. $X_{Hg} \approx 0.02$: P = 75 mW, SSW ~ 2, τ = 0.1 s. $X_{Hg} \approx 0.1$: P = 75 mW, SSW ~ 2.5, τ = 0.3 s. $X_{Hg} \approx 0.3$: P = 100 mW, SSW ~ 3.5, τ = 1 s. SR = 30 cm^{-1} min^{-1}.

shown the presence of linear triatomic molecules. In the molten state a molecular character has also been established for HgX_2 by a series of physicochemical measurements[28,29] including Raman spectroscopy.[30,31]

A recent reinvestigation[13] of the Raman spectra of HgX_2 (X = Cl, Br, I) in the liquid and solid states, with emphasis on the low-frequency region, confirmed the molecular character of these melts and indicated that due to intermolecular interactions the Raman-inactive vibrations of the linear HgX_2 molecule split in the liquid and become partially active in the spectra. As shown in Figures 1–3 the spectra of pure HgX_2 are dominated by a strong band with frequency corresponding to the Hg–X stretching[30,31] (marked as ν_1^S in Table II). A more detailed analysis of the assignment of the solvent bands listed in Table II will be given in ref 13.

In the solid state, mecury(I) (sub)halides Hg_2X_2 (X = F, Cl, Br, I) are also molecular containing linear tetraatomic molecules X–Hg–Hg–X having a metal–metal bond.[32] The Raman spectra of these solids show[33,34] strong bands at approximately 166, 134, and 113 cm^{-1} for the chloride, bromide, and iodide salts, respectively, which have been assigned to the Hg–Hg symmetric stretch (ν_2 (Σ_g^+)) of the Hg_2X_2 molecule. The frequencies of these bands correspond very well to the frequencies of the strong Raman bands observed in our spectra of the HgX_2–Hg mixtures and marked in Table II as ν_2^D. The symmetric stretch (Σ_g^+) frequencies[33,34] of the Hg_2X_2 molecules at approximately 279, 220, and 194 cm^{-1} also have a close correspondence to the weak bands measured in our spectra for each of the chloride, bromide, and iodide metal–molten salt mixtures (ν_1^D band in Table II). It is thus reasonable to assume that the observed Raman bands in the HgX_2–Hg melts, with low content of Hg, are mainly due to the formation of linear X–Hg–Hg–X molecules. As the chloride is substituted by bromide and by iodide, the ν_2^D frequency shifts to the red (Table II) as expected for a X–Hg–Hg–X molecule having the halogens bound to the Hg_2 group.

An additional proof for the formation of Hg_2Cl_2 molecules in these melts is given by studying the Raman spectra of melts containing mixed HgX_2–HgX'_2 halides and mercury metal. Figures 4 and 5 show representative spectra from these melts. Without the addition of metal the "solvent" mixtures give rise to new bands due to mixed X–Hg–X′ linear molecules. The main polarized Raman bands at 340 and 226 (HgClBr), 329 and 179 (HgClI), and 236 and 160 cm^{-1} (HgBrI) are in agreement with

(23) Gregg, A. H.; Hampson, G. C.; Jenkins, G. I.; Jones, P. L. F.; Sutton, L. G. *Trans. Faraday Soc.* **1937**, *33*, 852.
(24) Akishen, P. A.; Spiridonov, Y. P.; Khodchenkov, A. N. *Zh. Fiz. Khim.* **1959**, *33*, 20.
(25) Klemperer, W.; Lindeman, L. *J. Chem. Phys.* **1956**, *25*, 397.
(26) Klemperer, W. *J. Chem. Phys.* **1956**, *25*, 1066.
(27) Clark, R. J. H.; Rippon, D. M. *J. Chem. Soc., Faraday Trans.* **1973**, *69*, 1496.
(28) Janz, G. J.; McIntyre, J. D. E. *J. Electrochem. Soc.* **1962**, *109*, 842.
(29) Bockris, J. O. M.; Cook, E. H.; Bloom, H.; Richards, N. E. *Proc. R. Soc. London* **1960**, *A255*, 558.
(30) Janz, G. J.; James, D. W. *J. Chem. Phys.* **1963**, *38*, 902.
(31) Melveger, A. J.; Khanna, R. K.; Guscott, B. R.; Lippincott, E. R. *Inorg. Chem.* **1968**, *7*, 1630.
(32) (a) Havighurst, R. J. *J. Am. Chem. Soc.* **1926**, *48*, 2113. (b) Grdenic, D.; Djordjevic, J. *J. Chem. Soc.* **1956**, 1316. (c) Dorm, E. *Chem. Commun.* **1971**, 466.
(33) Richter, P. W.; Wong, P. T. T.; Whalley, E. *J. Chem. Phys.* **1977**, *67*, 2348 and references therein.
(34) During, J. R.; Lau, K. K.; Nagarajan, G.; Walker, M.; Bragin, J. *J. Chem. Phys.* **1969**, *50*, 2130.

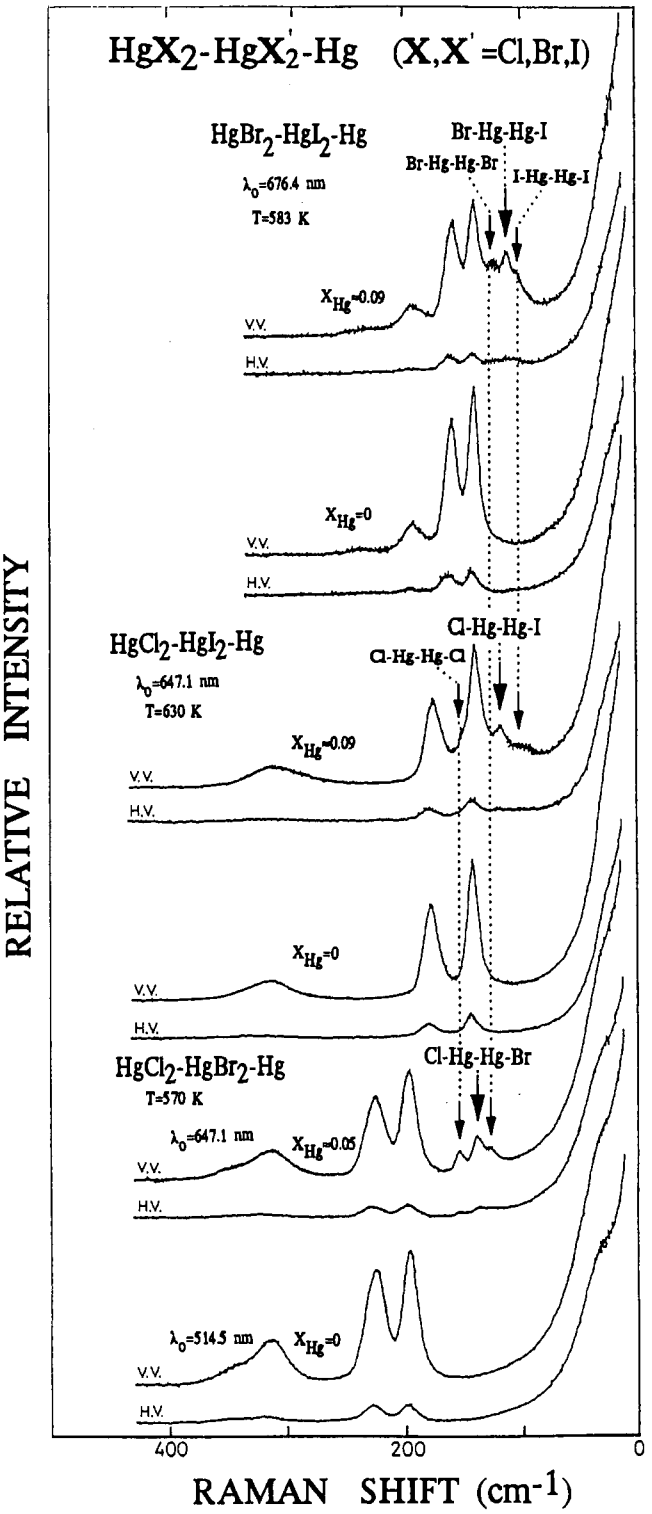

Figure 4. Raman spectra of the mixed HgX_2–HgX'_2–X (X ≠ X'; X, X' = Cl, Br, I) molten systems: SSW ~ 1.5, τ = 0.1 s, SR = 30 cm^{-1} min^{-1}. 53 mol % $HgCl_2$ + 47 mol % $HgBr_2$–Hg: P = 60 mW (X_{Hg} = 0), P = 160 mW ($X_{Hg} \approx 0.05$). 54 mol % $HgCl_2$ + 46 mol % HgI_2–Hg: P = 100 mW (X_{Hg} = 0), P = 160 mW ($X_{Hg} \approx 0.09$). 51 mol % $HgBr_2$ + 49 mol % HgI_2–Hg: P = 70 mW (X_{Hg} = 0), P = 160 mW ($X_{Hg} \approx 0.09$).

the values reported previously.[30,35] The fluorides are weak scatterers, and no HgFX (X = Cl, Br, I) bands were detected in the HgF_2–HgX_2 spectra. One exception was a weak band at ~460 cm^{-1}, which was present in the fluoride mixtures with chlorine or bromide and is attributed to the ν_{Hg-F} of the HgF_2 molecule.

The addition of Hg metal into a mixed halide solvent gives rise to three bands. Two bands correspond to ν_2^D frequencies observed previously (Figures 1–3) when mercury was dissolved separately in each of the component salts, and the third "new" band has an intermediate frequency between the two ν_2^D's. In Figure 4, for example, the spectra of $HgCl_2$–$HgBr_2$–Hg show the 154- and 124-cm^{-1} bands, which are also observed in the $HgCl_2$–Hg (Figure 1) and $HgBr_2$–Hg (Figure 2) systems as well as in other mixed halide solvents (see dotted lines in Figure 4). An intermediate band at 137 cm^{-1} is also present and is assigned to the stretching of the Cl–Hg–Hg–Br linear molecule. The systematic frequency changes of the "new" Raman bands observed for all the different mixed halide–mercury melts and their assignment are given in Table III.

In all the HgX_2–Hg mixtures having high metal concentrations (X_{Hg} > 0.15) a Raman band (ν^T in Table II) appears at frequencies below ν_2^D. The origin of the ν^T band is probably due to a polynuclear mercury species formed in these melts, and its red frequency shift with the substitution of Cl by Br or by I suggests that halides are bound to mercury. We have attributed this band to a stretching frequency of a Hg_3X_2 molecule. Linear Hg_3 chains bound to halides are expected[36] to have a stretching frequency in the range of frequencies where our ν^T values have been measured. Further support for this assignment is obtained from the spectra of the $Hg_3(AlCl_4)_2$ solid compound which is known to have a similar Hg_3 chain bound to two $AlCl_4$[37] and a Hg_3 stretching frequency in the range 93–123 cm^{-1}.[38] The Raman spectra of molten $Hg_3(AlCl_4)_2$ (Figure 6) show a predominant band at ~85 cm^{-1}, which is close to the ~100-cm^{-1} band of the metal-rich $HgCl_2$–Hg mixtures. Presumably, both bands have as common origin the Hg_3 chain, and the shift of ~10–15 cm^{-1} on going from Hg_3Cl_2 to $Hg_3(AlCl_4)_2$ reflects the mass increase of the terminal "units" ($AlCl_4^-$ or Cl^-) bound to Hg_3.

From the spectra in Figures 1–3 it can be seen that the addition of Hg shifts the Hg–X vibrational frequency (ν_1^S) of the solvent HgX_2 molecule toward the red. The effect is more pronounced for the chloride melts where the ν_1^S(Ag) mode from ~310 cm^{-1} in pure $HgCl_2$ shifts to ~295 cm^{-1} for X_{Hg} = 0.3. Similar red shifts have been observed in the spectra of $HgCl_2$–ACl (A = NH_4, K)[39] and $HgCl_2$–CsCl[13] binary melts and have been attributed to the formation of ionic species of the type $HgCl_3^-$ ($\nu_{Hg-Cl} \approx 280$ cm^{-1}) and $HgCl_4^{2-}$ ($\nu_{Hg-Cl} \approx 265$ cm^{-1}) which are stabilized in the alkali-metal chloride rich mixtures. For a molecular mixture composed of $HgCl_2$ and Hg_2Cl_2 molecules the presence of ionic species seems unlikely. The self-ionization scheme suggested by Janz[28] [$2HgCl_2 \leftrightarrow HgCl_3^- + HgCl^+$] could to some extent take place and even be enhanced by the formation of Hg_2Cl^+ species in melts containing mercury metal. The absence however from the Raman spectra of any bands due to $HgCl^+$, Hg_2Cl^+, ... excludes the formation of ionic species in considerable amounts and cannot account for the red shift of the ν_1^S band. Another possibility is that the red shift might be due to intermolecular interactions between the $HgCl_2$ and Hg_2Cl_2 molecules. The mercury atom(s) within the linear molecules can easily have as nearest neighbors the terminal chloride(s) from neighboring molecules. This is shown schematically in Figure 7 for a "latticelike" two-dimensional mixture where the Hg atoms of a Hg_2X_2 molecule are rather close to the X atoms of neighboring HgX_2 molecules. The mercury-neighboring halide interaction between the HgX_2–Hg_2X_2 molecules results in weak "network" type interactions in the mixture and reflects a weakening of the Hg–X bond in both molecules, giving rise to the red shift seen in our spectra for the ν_1^S and to some extent for the ν_2^D bands. These interactions could favor exchange of halides with *alternation* of oxidation states between neighboring molecules (Figure 7). In the three-dimensional liquid mixture the number of nearest neighbors around each molecule

(35) Clark, J. H. R.; Solomons, C. *J. Chem. Phys.* **1968**, *48*, 528.

(36) Cutforth, B. D.; Davies, C. G.; Dean, P. A. W.; Gillespie, R. J.; Ireland, P. R.; Ummat, P. K. *Inorg. Chem.* **1973**, *12*, 1343.

(37) Ellison, R. D.; Levy, H. A.; Fung, K. W. *Inorg. Chem.* **1972**, *11*, 833.

(38) Torsi, G.; Fung, K. W.; Begun, G. M.; Mamantov, G. *Inorg. Chem.* **1971**, *10*, 2285.

(39) Janz, G. J.; James, D. W. *J. Chem. Phys.* **1963**, *38*, 905.

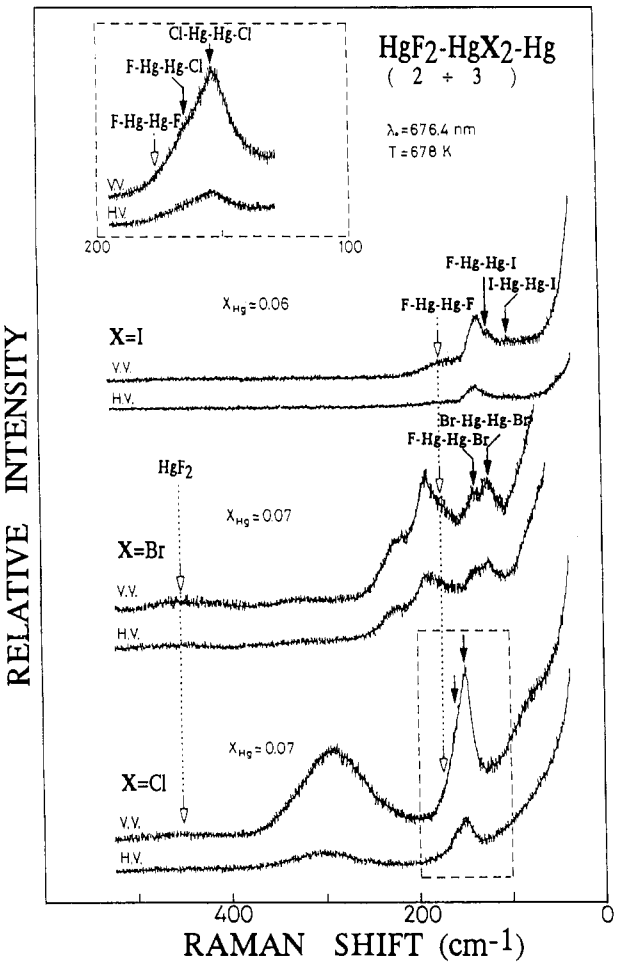

Figure 5. Raman spectra of the mixed HgF_2–HgX_2–Hg (X = Cl, Br, I) molten systems. X = Cl: P = 90 mW, SSW ~ 1, τ = 1 s, SR = 15 cm^{-1} min^{-1}. X = Br: P = 120 mW, SSW ~ 2.5, τ = 0.3 s, SR = 30 cm^{-1} min^{-1}. X = I: P = 140 mW, SSW ~ 3.5, τ = 0.3 s, SR = 30 cm^{-1} min^{-1}. Insert X = Cl: P = 140 mW, SSW ~ 0.5, τ = 2 s, SR = 1.2 cm^{-1} min^{-1}.

Table III. Symmetric Stretching Frequency (ν_2^D, cm^{-1}) of the linear X–Hg–Hg–X′ Molecules

molecule	ν_2^D(Hg–Hg)	molecule	ν_2^D(Hg–Hg)
F–Hg–Hg–F	180	F–Hg–Hg–I	128
F–Hg–Hg–Cl	170	Br–Hg–Hg–Br	124
Cl–Hg–Hg–Cl	154	Cl–Hg–Hg–I	118
F–Hg–Hg–Br	142	Br–Hg–Hg–I	112
Cl–Hg–Hg–Br	137	I–Hg–Hg–I	100

increases and the neighboring halide–mercury interactions are more likely. Thus halide exchange and alternation of oxidation states should occur easier in the real three-dimensional liquid than in the two-dimensional latticelike model.

The mechanism proposed here is compatible and gives some understanding of the drastic electrical conductivity changes occurring when Hg is added to HgX_2 (X = Cl, I).[16] For example, pure $HgCl_2$ behaves as an insulator having conductivity $\kappa_{400K} \approx 1.1 \times 10^{-3}$ $(\Omega \cdot cm)^{-1}$ in the range expected for molecular liquids. The addition of Hg increases the conductivity gradually but not linearly and at $X_{Hg} \approx 0.3$ and $\kappa_{400K} \approx 1.1 \times 10^{-1}$ $(\Omega \cdot cm)^{-1}$, a value that is lower than that expected for ionic conduction [<5–6 $(\Omega \cdot cm)^{-1}$] but of the same order of magnitude as the values measured for hopping semiconductors. Thus it seems that the intermolecular interactions in the melt mixture and the suggested mechanism give an account for the intermediate values of conductivities and indicate that a "hopping" like conduction contributes to the conductivity of these liquid mixtures.

Similar intermediate values in conductivity have been noted in certain molten mixtures containing salts which, as pure components, are known to behave like molecular liquids. Poulsen and Bjerrum[40] have measured anomalous ionic-like conductivities in molten $BiCl_3$–$AlCl_3$, $TeCl_4$–$AlCl_3$, and KCl–$TeCl_4$ mixtures and have interpreted their data in terms of a Grotthus-type chloride-transfer mechanism between labile donor and acceptor units simultaneously present in the melt. A chloride-exchange transport process has been also proposed by Mamantov and co-workers,[41] in order to account for the conductivity data of the $SbCl_3$–$AlCl_3$–KCl mixture. The above suggested mechanism for the HgX_2–Hg melts involves a chloride-exchange as well as an interchange of oxidation states between the HgX_2 and Hg_2X_2 molecule.

Finally, it should be noted that weak ionization of Hg_2X_2 in the melt mixture forming ionic species (e.g. Hg_2X^+) with con-

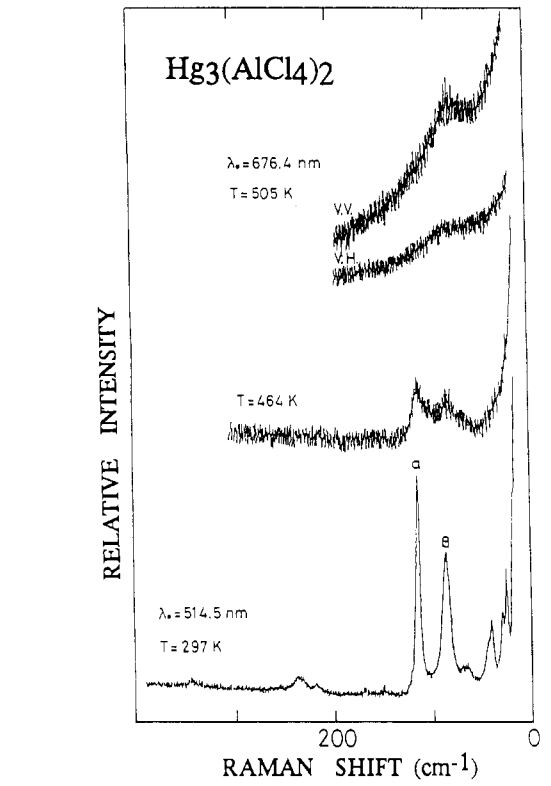

Figure 6. Raman spectra of the $Hg_3(AlCl_4)_2$ compound. Solid: [T = 297 K] P = 40 mW, SSW ~ 2, τ = 0.1 s; [T = 464 K] P = 50 mW, SSW ~ 3, τ = 0.3 s. Liquid: [T = 505 K] P = 80 mW, SSW ~ 2, τ = 0.3 s. SR = 30 cm^{-1} min^{-1}. The α and β doublet in the solid is attributed to a factor group splitting of the Hg_3^{2+} symmetrical stretch.[36]

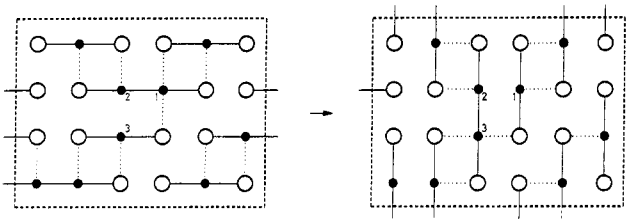

Figure 7. Schematic two-dimensional "latticelike" model of the HgX_2–Hg_2X_2 molecular mixture. Dotted lines indicate Hg–X interactions between neighboring molecules. The alternation of oxidation states is depicted with mercury atoms 1–3. In the left side atom 1 is subvalent and atom 3 divalent, while in the right side atom 1 is divalent and atom 3 subvalent. It is noteworthy that in the solid state[19,32] the two Hg–X intermolecular distances for HgX_2 and Hg_2X_2 are not much different (e.g. for $HgCl_2$ the distance between two linear and parallel molecules is 3.42 Å, while the corresponding distance for Hg_2Cl_2 is 3.21 Å).

(40) Poulsen, F. W.; Bjerrum, N. J. *J. Phys. Chem.* **1975**, *79*, 1610.
(41) Petrovic, C.; Mamantov, G.; Sorlie, M.; Lietzke, M. L.; Smith, G. P. *J. Phys. Chem.* **1982**, *86*, 4598.

centrations too low to be detected by Raman spectroscopy cannot be excluded. Such an ionization could also contribute to the conductivity of these mixtures.

Acknowledgment. This work has been supported by the Hellenic General Secretariat of Research and Technology and the EEC "SCIENCE" program.

Registry No. Hg, 7439-97-6; $HgCl_2$, 7487-94-7; $HgBr_2$, 7789-47-1; HgI_2, 7774-29-0; HgF_2, 7783-39-3; $Hg_3(AlCl_4)_2$, 36554-82-2.

Contribution from the Heavy Water Division, Bhabha Atomic Research Centre, Bombay 400085, India

Electronegativity, Hardness, and Chemical Binding in Simple Molecular Systems

Tapan K. Ghanty and Swapan K. Ghosh*

Received September 16, 1991

A new electronegativity-based approach to chemical binding is proposed where the covalent binding is formulated in terms of the accumulation of electron density at the bond center using the concepts of bond electronegativity and bond hardness. In an AB_n type molecule, the covalent contribution to the single A-B bond energy is shown to be given by a simple expression in terms of the A-A and B-B bond energies. For heteronuclear diatomic molecules, this reduces to an average of the geometric and arithmetic means of the bond energies of corresponding homonuclear diatomics. This covalent part together with the derived expression for the ionic contribution with no adjustable parameter constitutes the total bond energy expression. Predicted numerical results on bond energies and atomic charges of selected diatomic and simple polyatomic molecules are shown to agree well with available data.

Introduction

The concept of electronegativity, introduced originally by Pauling[1] and Mulliken,[2] has played a fundamental role in the conceptual development of all branches of chemistry.[3] The electronegativity defined as

$$\chi = -(\partial E/\partial N) \tag{1}$$

originally due to Pritchard and Sumner[4] as well as Iczkowski and Margrave[5] denotes the energy derivative with respect to number of electrons and is equal to $(I + A)/2$ in a finite difference approximation, where I and A represent ionization potential and electron affinity, respectively. This concept now rests on a profound theoretical basis within the framework of density functional theory[6] due to the work of Parr et al.,[7] who identified χ as the negative of the chemical potential μ of the electron cloud, viz.

$$\chi = -\mu = -(\delta E/\delta \rho) \tag{2}$$

where the functional derivative is with respect to the electron density $\rho(r)$. This definition provides not only a means of quantum mechanical calculation of χ but also a justification for the electronegativity equalization procedure used widely in chemistry.[3]

Another important quantity is the second derivative of energy identified[8] recently as a measure of chemical hardness[9]

$$\eta = \tfrac{1}{2}(\partial^2 E/\partial N^2) = \tfrac{1}{2}(\partial \mu/\partial N) \tag{3}$$

which equals $(I - A)/2$ in a finite difference approximation but can also be expressed in terms of electron density[10] and is thus amenable to a quantum mechanical calculation.

An understanding or prediction of molecule formation in terms of these atomic properties has been of much importance in chemistry. The electronegativity parameter governs the charge transfer in chemical binding and hence determines the polarity of the molecule. The binding energy of a molecule however consists of not only this charge-transfer contribution but also the energy involved in covalent bond formation—the latter being the only contribution for homonuclear molecules.

For a diatomic molecule AB, Pauling[1] has proposed that the covalent contribution can be approximated as the geometric mean of the corresponding homopolar bond energies, i.e.

$$D_{AB}^{cov} = (D_{AA}D_{BB})^{1/2} \tag{4}$$

and thus led to the bond energy equation[1]

$$D_{AB} = D_{AB}^{cov} + 30(\chi_A - \chi_B)^2 \tag{5}$$

where the last term denotes the energy (in kcal/mol) associated with the charge-transfer process.

Several other empirical equations have later been proposed; e.g., Matcha[11] has prescribed an equation of the form

$$D_{AB} = D_{AB}^{cov} + K\{1 - \exp[-(30/K)(\chi_A - \chi_B)^2]\} \tag{6}$$

with the empirical parameter K being equal to 103 for energy expressed in kcal/mol. Reddy et al.[12] have recently proposed a very simple formula of the form

$$D_{AB} = D_{AB}^{cov} + 32.058|\chi_A - \chi_B| \tag{7}$$

In eqs 4-7, D_{AB}^{cov} denotes the full covalent contribution to the bond energy. Sanderson[13] and Huheey,[14] however, have treated the

(1) Pauling, L. *The Nature of the Chemical Bond*, 3rd ed.; Cornell University Press: Ithaca NY, 1960.
(2) Mulliken, R. S. *J. Chem. Phys.* **1934**, *2*, 782-793.
(3) Sen, K. D., Jorgensen, C. K., Eds. *Electronegativity: Structure and Bonding*; Springer-Verlag: Berlin, 1987; Vol. 66.
(4) Pritchard, H. O.; Sumner, F. H. *Proc. R. Soc. London* **1956**, *A235*, 136-143.
(5) Iczkowski, R. P.; Margrave, J. L. *J. Am. Chem. Soc.* **1961**, *83*, 3547-3551.
(6) Parr, R. G.; Yang, W. *Density Functional Theory of Atoms and Molecules*; Oxford University Press: New York, 1989.
(7) Parr, R. G.; Donnelly, R. A.; Levy, M.; Palke, W. E. *J. Chem. Phys.* **1978**, *68*, 3801-3807.
(8) Parr, R. G.; Pearson, R. G. *J. Am. Chem. Soc.* **1983**, *105*, 7512-7516.
(9) Pearson, R. G. *Hard and Soft Acids and Bases*; Dowden, Hutchinson, and Ross: Stroudsville, PA, 1973.
(10) Berkowitz, M.; Ghosh, S. K.; Parr, R. G. *J. Am. Chem. Soc.* **1985**, *107*, 6811-6814. Ghosh, S. K. *Chem. Phys. Lett.* **1990**, *172*, 77-82.
(11) Matcha, R. L. *J. Am. Chem. Soc.* **1983**, *105*, 4859-4862.
(12) Reddy, R. R.; Rao, T. V. R.; Biswanath, R. *J. Am. Chem. Soc.* **1989**, *111*, 2914-2915.
(13) Sanderson, R. T. *Chemical Bonds and Bond Energy*; Academic: New York, 1976. Sanderson, R. T. *Polar Covalence*; Academic: New York, 1983.
(14) Huheey, J. E. *Inorganic Chemistry*, 3rd ed.; Harper & Row: New York, 1983.

0020-1669/92/1331-1951$03.00/0